Nd^{3+}, Ho^{3+}-codoped apatite-related $NaLa_9(GeO_4)_6O_2$ phosphors for the near- and middle-infrared region

Yana V. Baklanova,[a] Olga A. Lipina,[a] Andrey N. Enyashin,[a] Ludmila L. Surat,[a] Alexander P. Tyutyunnik,[a] Nadezda V. Tarakina,[b,c] A. Dominic Fortes,[d] Alexander Yu. Chufarov,[a] Evgeny V. Gorbatov[a] and Vladimir G. Zubkov[a]

[a] Institute of Solid State Chemistry, UB RAS, 620990 Ekaterinburg, Russia.
[b] Max Planck Institute of Colloids and Interfaces, Am Mühlenberg 1, 14476 Potsdam, Germany.
[c] School of Engineering and Materials Science, Queen Mary University of London, Mile End Road, London E1 4NS, United Kingdom.
[d] ISIS Facility, Rutherford Appleton Laboratory, Harwell Science & Innovation Campus, Chilton, Oxfordshire OX11 0QX, United Kingdom.

Supplementary Information

Table S1. Crystal data for $NaLa_{9-x-y}Nd_xHo_y(GeO_4)_6O_2$ powders

x	*y*	*a*, Å	*c*, Å	*V*, Å^3
0.025	2×10^{-7}	9.8887(4)	7.2621(4)	614.99(3)
0.050	3×10^{-7}	9.8892(4)	7.2613(4)	614.99(3)
0.075	4×10^{-7}	9.8882(4)	7.2615(4)	614.89(3)
0.100	5×10^{-7}	9.8884(4)	7.2606(4)	614.83(3)
0.125	6×10^{-7}	9.8875(4)	7.2611(4)	614.77(3)
0.125	1.4×10^{-6}	9.8875(4)	7.2594(4)	614.62(3)
0.150	7×10^{-7}	9.8877(4)	7.2597(4)	614.67(3)
0.200	8×10^{-7}	9.8871(4)	7.2592(4)	614.54(3)
0.125	0.01	9.8855(4)	7.2625(4)	614.63(3)
0.125	0.10	9.8859(4)	7.2553(4)	614.07(3)

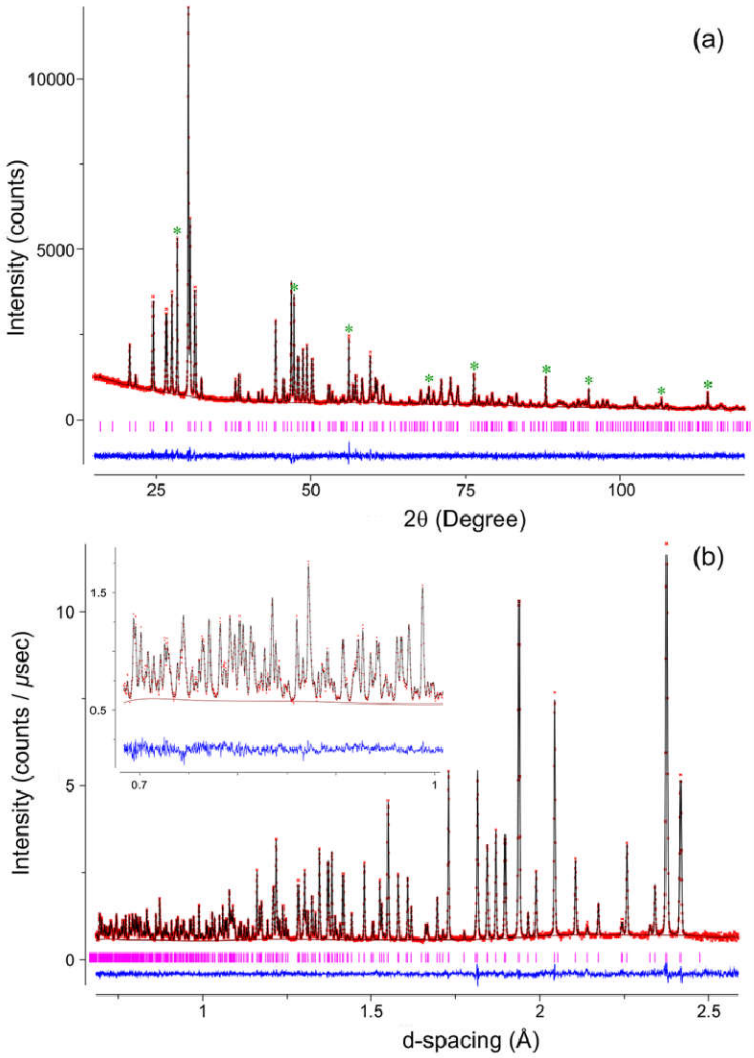

Fig. S1. Experimental, calculated, and difference patterns of $NaLa_{8.875-y}Nd_{0.125}Ho_y(GeO_4)_6O_2$ ($y = 1.4\times10^{-6}$): (a) XRD, (b) TOF NPD. The symbol "*" denotes the peaks of the internal silicon standard.

Table S2. Structural data for $NaLa_{8.875-y}Nd_{0.125}Ho_y(GeO_4)_6O_2$ ($y = 1.4\times10^{-6}$) based on neutron data

Space group, #	$P6_3/m$, 176
The number of formula units, Z	1
Cell constants:	
$a = b$, Å	9.88903(6)
c, Å	7.25602(5)
V, Å^3	614.521(7)
D_x, g/cm^3	5.757
wRp, %	2.25
Rp, %	2.98
R(F^2), %	3.99
χ^2	1.930

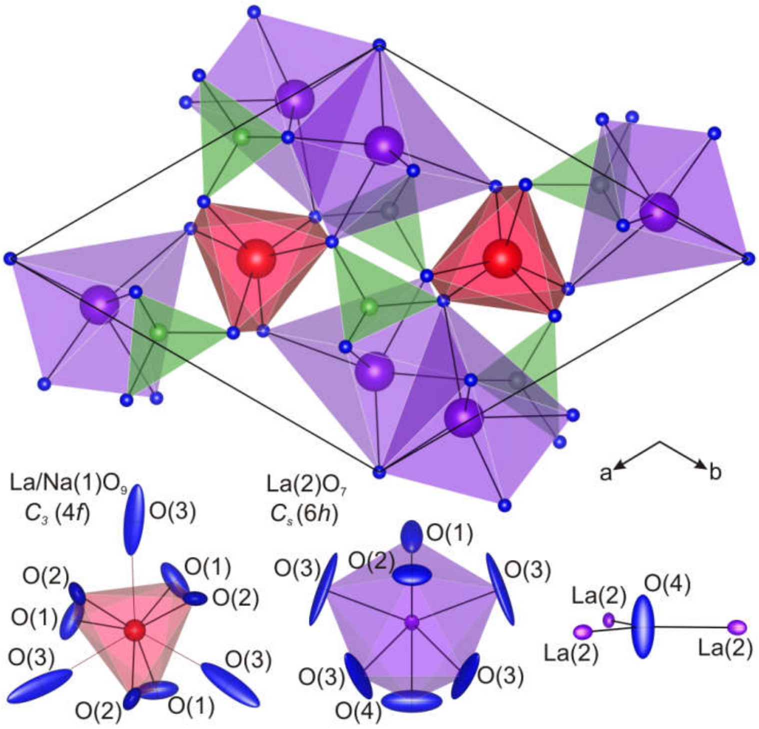

Fig. S2. Projections of the crystal structure of $NaLa_{8.875-y}Nd_{0.125}Ho_y(GeO_4)_6O_2$ ($y = 1.4\times10^{-6}$) onto the (001) planes: GeO_4 tetrahedra (green), La/Na(1)O_9 twisted trigonal prisms (red), La(2)O_7 polyhedra (purple) and oxygen atoms (blue balls), and the coordination environment of cation positions.

Table 3. Atomic coordinates and anisotropic thermal parameters (U × 100, Å^2) of $NaLa_{8.875-y}Nd_{0.125}Ho_y(GeO_4)_6O_2$ ($y = 1.4\times10^{-6}$) based on neutron data

Atom		*x/a*	*y/b*	*z/c*	Fraction	U11×100	U22×100	U33×100	U12×100	U13×100	U23×100
La/ Na/ Nd(1)	4*f*	1/3	2/3	-0.00052(13)	0.7396/ 0.25/ 0.0104	0.73(3)	0.73(3)	1.29(5)	0.36(2)	0	0
La/ Nd(2)	6*h*	0.24175(6)	0.01243(8)	1/4	0.9861/ 0.0139	0.39(4)	0.23(3)	0.31(3)	0.01(3)	0	0
Ge	6*h*	0.37354(7)	0.40133(7)	1/4	1.0	0.33(3)	0.53(3)	0.42(3)	0.32(3)	0	0
O(1)	6*h*	0.48858(10)	0.31495(10)	1/4	1.0	1.50(6)	2.83(6)	0.72(5)	1.76(5)	0	0
O(2)	6*h*	0.52442(10)	0.39596(10)	3/4	1.0	0.34(5)	0.66(5)	2.31(6)	0.05(4)	0	0
O(3)	12*i*	0.24763(8)	0.33958(9)	0.43834(7)	1.0	1.52(4)	7.61(6)	1.18(3)	2.83(4)	1.10(3)	2.68(4)
O(4)	2*a*	0.0	0.0	1/4	1.0	0.72(5)	0.72(5)	5.41(13)	0.36(2)	0	0

Anisotropic thermal factors are defined by $T = e\,[-2\pi^2(u_{11}h^2a^{*2} + \ldots + 2u_{12}hka^*b^* + \ldots)]$

Table S4. Selected interatomic distances d (Å) and angles (°) for $NaLa_{8.875-y}Nd_{0.125}Ho_y(GeO_4)_6O_2$ ($y = 1.4\times10^{-6}$) based on neutron data

Interatomic distances		Interatomic distances	
M(1)-O(1) ×3	2.4681(9)	M(2)-O(1)	2.7578(11)
M(1)-O(2) ×3	2.5569(10)	M(2)-O(2)	2.5282(10)
M(1)-O(3) ×3	2.9399(7)	M(2)-O(3) ×2	2.6203(9)
M(1)-O[b]	**2.6549**	M(2)-O(3) ×2	2.4306(6)
Expected[a]	2.597	M(2)-O(4)	2.3317(5)
		M(2)-O[b]	**2.5314**
Ge-O(1)	1.7308(9)	Expecteda	2.470
Ge-O(2)	1.7360(9)		
Ge-O(3) ×2	1.7408(7)		
Ge-O	**1.7371**		
Expected[a]	1.770		
Angles		Angles	
O(1)-M(1)-O(1) ×3	72.13(3)	O(1)-M(2)-O(2)	98.47(3)
O(1)-M(1)-O(2) ×3	94.62(2)	O(1)-M(2)-O(3) ×2	145.49(2)
O(1)-M(1)-O(2) ×3	154.41(3)	O(1)-M(2)-O(3) ×2	69.87(2)
O(1)-M(1)-O(2) ×3	125.58(2)	O(1)-M(2)-O(4)	112.66(3)
O(2)-M(1)-O(2) ×3	75.04(3)	O(2)-M(2)-O(3) ×2	85.76(2)
		O(2)-M(2)-O(3) ×2	70.12(3)
O(1)-Ge-O(2)	115.08(6)	O(2)-M(2)-O(4)	148.88(4)
O(1)-Ge-O(3) ×2	110.99(3)	O(3)-M(2)-O(3)	62.87(3)
O(2)-Ge-O(3) ×2	107.81(4)	O(3)-M(2)-O(3)	137.00(4)
O(3)-Ge-O(3)	103.45(5)	O(3)-M(2)-O(3) ×2	76.74(1)
		O(3)-M(2)-O(3) ×2	137.82(3)
		O(4)-M(2)-O(3) ×2	83.49(2)
		O(4)-M(2)-O(3) ×2	104.41(2)

[a] The sum of the crystal radii according to[47]: Na^+ IX – 1.380 Å;La^{+3} VII – 1.24 Å, La^{+3} IX – 1.356 Å; Nd^{+3} VII – 1.186 Å was calculated as mean of Nd^{+3} VI – 1.123, Nd^{+3} VIII – 1.249, and Nd^{+3} IX – 1.303 Å; Ge^{+4} IV – 0.530 Å,;O^{-2} III – 1.22 Å, O^{-2} IV – 1.24 Å. Effective crystal radius was calculated taking in account fractions.

[b] The average values are indicated by boldface type. M(1) = La/Na/Nd(1), M(2) = La/Nd(2).

Table S5. Bond–valence sums (BVSs) for the cations and oxygen anions for $NaLa_{8.875-y}Nd_{0.125}Ho_y(GeO_4)_6O_2$ ($y = 1.4\times10^{-6}$)

Atom	Assumed oxidation state	BVS	% deviation
La(1)	+3	2.793	7
Na(1)	+1	1.011	1
La(2)	+3	2.834	6
Ge	+4	4.130	3
O(1)	-2	1.971	1
O(2)	-2	2.014	1
O(3)	-2	1.928	4
O(4)	-2	1.953	2

BVSs were calculated taking into account La/Na fractions, fractions of Nd were added to fraction of La.

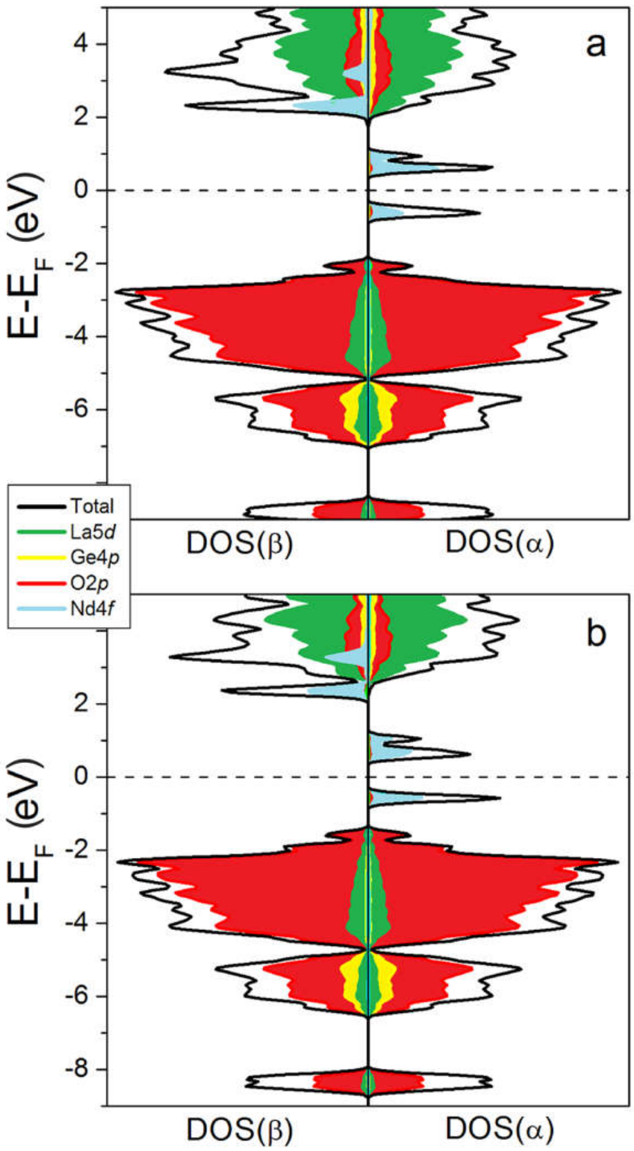

Fig. S3. Spin-resolved total and partial densities of states (DOS) for the $NaLa_9(GeO_4)_6O_2$ compound doped by single-atom Nd impurities on 6*h* (a) or 4*f* sites (b). DFT GGA calculations.

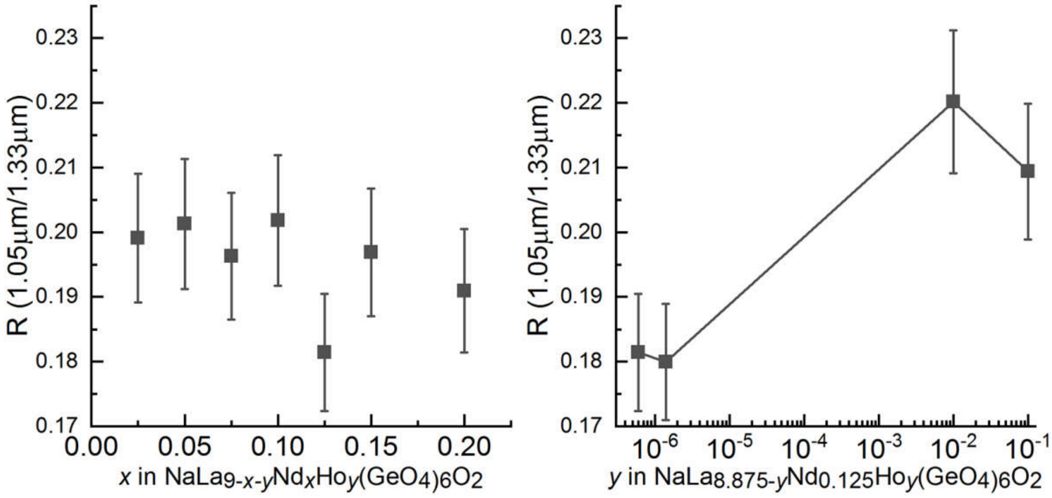

Fig. S4. The ratios of the integrated intensities of lines centered at 1.05 μm and 1.33 μm depend on the Nd^{3+} and Ho^{3+} concentration in the $NaLa_{9-x-y}Nd_xHo_y(GeO_4)_6O_2$ (x = 0.025–0.200, $y = 2\times10^{-7}$–0.1).

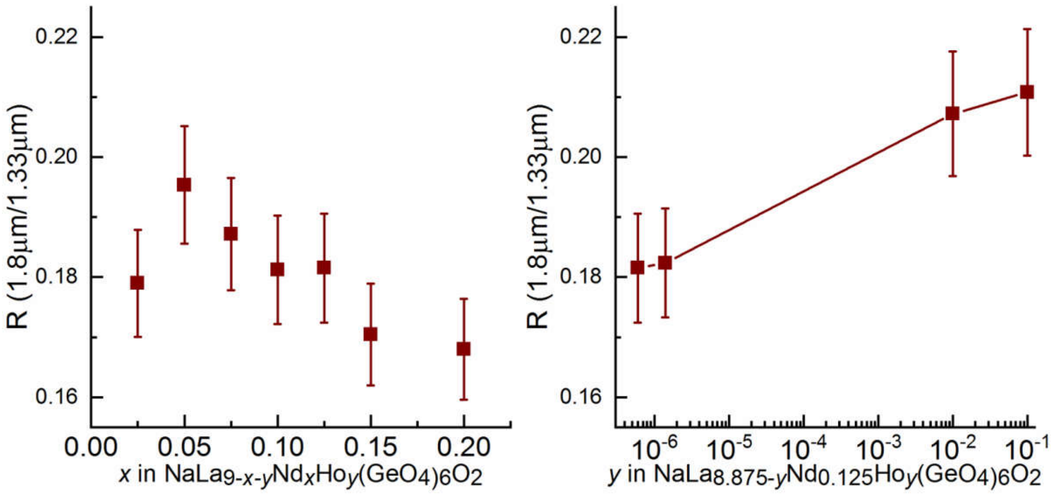

Fig. S5. The ratios of the integrated intensities of lines centered at 1.33 μm and 1.80 μm depend on the Nd^{3+} and Ho^{3+} concentration in the $NaLa_{9-x-y}Nd_xHo_y(GeO_4)_6O_2$ (x = 0.025–0.200, $y = 2\times10^{-7}$–0.1).

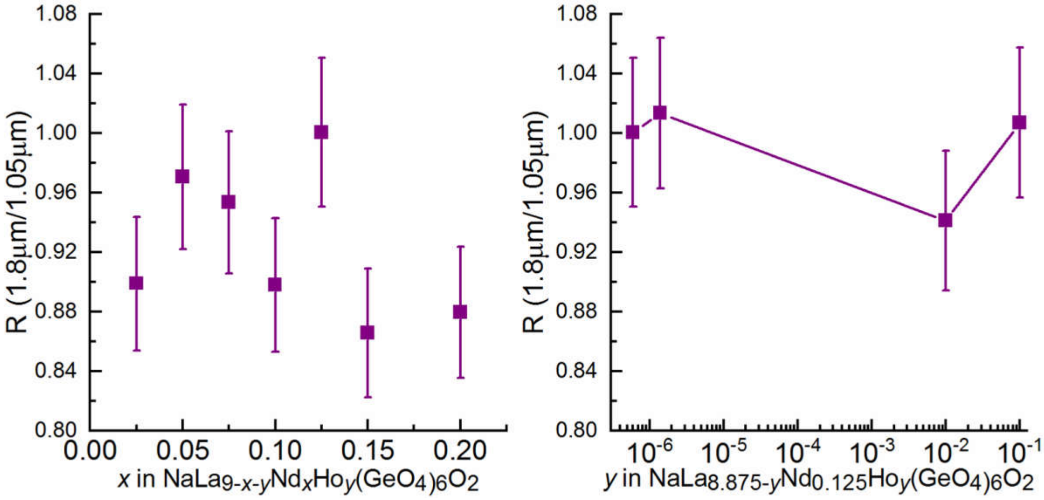

Fig. S6. The ratios of the integrated intensities of lines centered at 1.05 µm and 1.80 µm depend on the Nd^{3+} and Ho^{3+} concentration in the $NaLa_{9\text{-}x\text{-}y}Nd_xHo_y(GeO_4)_6O_2$ (x = 0.025–0.200, y = 2×10^{-7}–0.1).

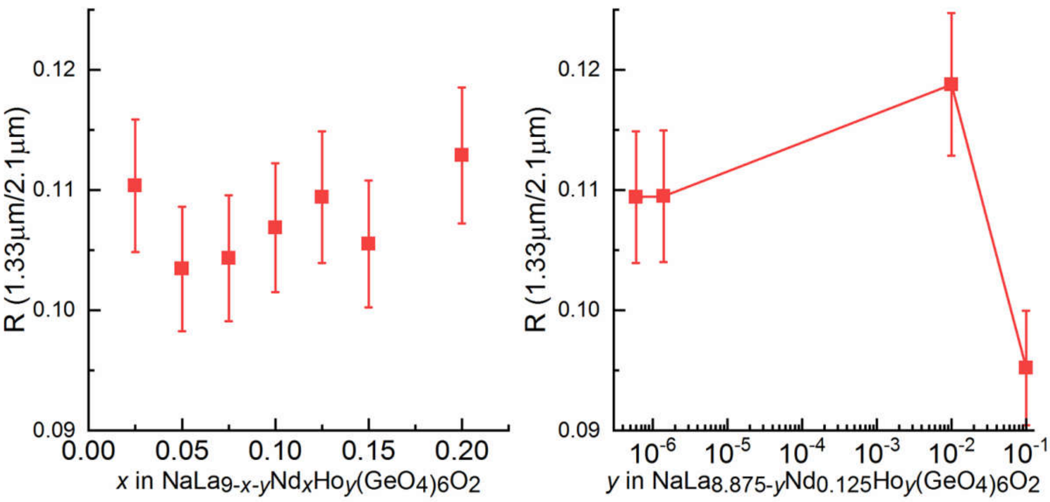

Fig. S7. The ratios of the integrated intensities of lines centered at 1.33 µm and 2.10 µm depend on the Nd^{3+} and Ho^{3+} concentration in the $NaLa_{9\text{-}x\text{-}y}Nd_xHo_y(GeO_4)_6O_2$ (x = 0.025–0.200, y = 2×10^{-7}–0.1).

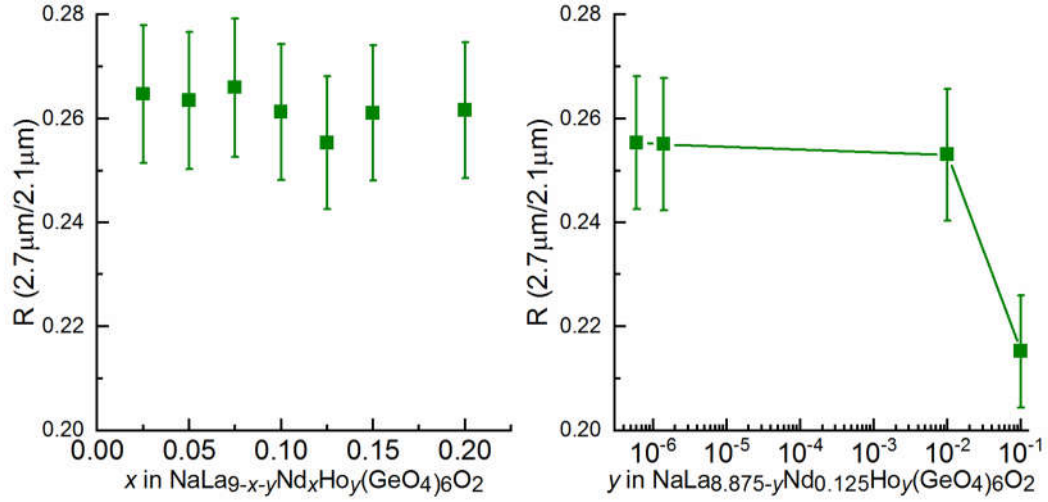

Fig. S8. The ratios of the integrated intensities of lines centered at 2.1 μm and 2.7 μm depend on the Nd^{3+} and Ho^{3+} concentration in the $NaLa_{9-x-y}Nd_xHo_y(GeO_4)_6O_2$ ($x = 0.025$–0.200, $y = 2\times10^{-7}$–0.1).

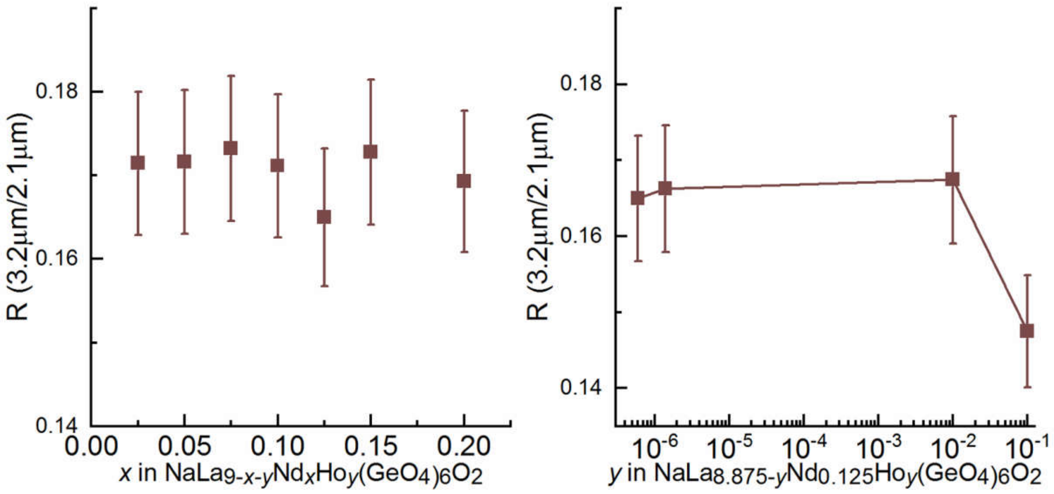

Fig. S9. The ratios of the integrated intensities of lines centered at 2.1 μm and 3.2 μm depend on the Nd^{3+} and Ho^{3+} concentration in the $NaLa_{9-x-y}Nd_xHo_y(GeO_4)_6O_2$ ($x = 0.025$–0.200, $y = 2\times10^{-7}$–0.1).

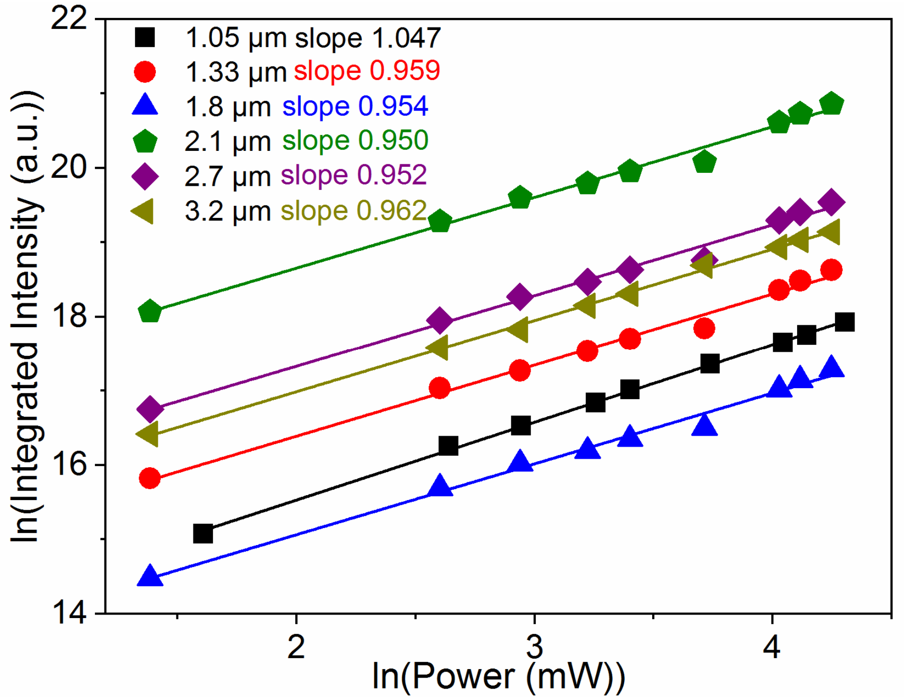

Fig. S10. The power dependences of the luminescence intensity of the lines at 1.05 μm, 1.33 μm, 1.80 μm, 2.10 μm, 2.70 μm and 3.20 μm for the $NaLa_{8.875-y}Nd_{0.125}Ho_y(GeO_4)_6O_2$ (y = 1.4×10^{-6}) sample at the low-power regime. The laser excitation wavelength is 808 nm.

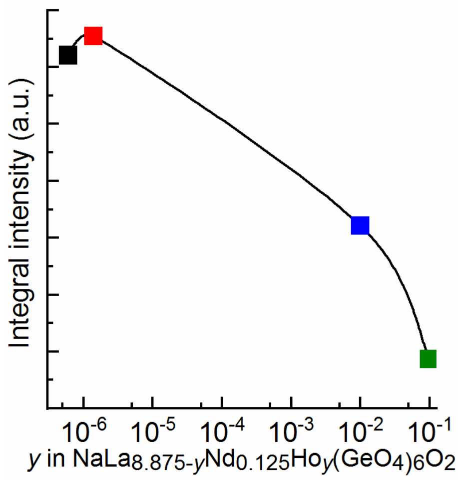

Fig. S11. The integral luminescence intensity of the 3.2 μm lines versus Ho^{3+} concentration in $NaLa_{8.875-y}Nd_{0.125}Ho_y(GeO_4)_6O_2$ (y = 6×10^{-7}–0.1).